Sub-additive ionic transport across arrays of solid-state nanopores

A. Gadaleta, C. Sempere, Simon Gravelle, Alessandro Siria, R. Fulcrand, C. Ybert, Lydéric Bocquet

PHYSICS OF FLUIDS **26**, 012005 (2014)

Sub-additive ionic transport across arrays of solid-state nanopores

A. Gadaleta,[1,a)] C. Sempere,[1,a)] S. Gravelle,[1] A. Siria,[1] R. Fulcrand,[1] C. Ybert,[1] and L. Bocquet[1,2,3,a)]
[1]*ILM, Université Lyon 1 and CNRS, UMR 5306, F-69622 Villeurbanne, France*
[2]*Department of Civil and Environmental Engineering, Massachusetts Institute of Technology, Cambridge, Massachusetts 02139, USA*
[3]*UMI 3466 CNRS-MIT, Massachusetts Institute of Technology, Cambridge, Massachusetts 02139, USA*

(Received 21 September 2013; accepted 11 January 2014; published online 31 January 2014)

Nanopores, either biological, solid-state, or ultrathin pierced graphene, are powerful tools which are central to many applications, from sensing of biological molecules to desalination and fabrication of ion selective membranes. However, the interpretation of transport through low aspect-ratio nanopores becomes particularly complex as 3D access effects outside the pores are expected to play a dominant role. Here, we report both experiments and theory showing that, in contrast to naïve expectations, long-range mutual interaction across an array of nanopores leads to a non-extensive, sub-linear scaling of the global conductance on the number of pores N. A scaling analysis demonstrates that the N-dependence of the conductance depends on the topology of the network. It scales like $G \sim N/\log N$ for a 1D line of pores, and like $G \sim \sqrt{N}$ for a 2D array, in agreement with experimental measurements. Our results can be extended to alternative transport phenomena obeying Laplace equations, such as diffusive, thermal, or hydrodynamic transport. Consequences of this counter-intuitive behavior are discussed in the context of transport across thin membranes, with applications in energy harvesting. © *2014 AIP Publishing LLC*. [http://dx.doi.org/10.1063/1.4863206]

I. INTRODUCTION

Solid-state nanopore membranes are well-known for their powerful applications in multiple domains, in particular in biology, as low-cost biosensors,[1] but also in engineering as devices for filtering or for the generation of energy.[2,3] A biosensor is made of a nanopore connected to two fluid reservoirs, between which a potential or pressure drop is imposed. The particles in solution are driven through the nanopore, where their passage temporarily blocks the flow of ionic current. It is thus possible to detect biological components, such as proteins, by measuring the ionic current crossing the nanopore.[4–8] This is expected to achieve fast and low-cost sequencing of DNA.[1] Furthermore, in the context of desalination or energy conversion, *multi-pore* membranes also raise great hopes to increase the efficiency of the process.[9,10] The passage through the ultrathin nanopores is a key to their unique properties: it provides high sensitivity to molecular passage, as well as enabling the building up of huge potential and chemical gradients across the thin membranes which facilitates the passage.[11] In this context, pierced graphene constitutes the ultimate membrane, yielding great expectations for applications.[12–15]

Success in using nanopores lies in a proper understanding of transport properties of molecules, but also of ionic current signals through the nanopores, which is commonly used as a probe of macromolecule transport. It has been known since the 1960s that ionic transport through thin pores

[a)]A. Gadaleta, C. Sempere, and L. Bocquet contributed equally to this work.

is dominated by access effects occurring at the entrance of the nanopore. Hille,[16] followed by Hall,[17] first calculated the access resistance through a small circular pore in a membrane, by using an analogy to an electrostatic capacitance problem. The total conductance is written accordingly as[18]

$$G = (R_{\text{channel}} + 2R_{\text{access}})^{-1} = \kappa_b \left[\frac{4l}{\pi d^2} + \frac{1}{d} \right]^{-1} \tag{1}$$

with κ_b the bulk ionic conductivity, l the pore length, and d its diameter. More sophisticated approaches, solving explicitly the Poisson-Nernst-Planck equations,[19] do not predict appreciable deviations from Hall's[17] formula, at least in neutral or weakly charged membranes.[20] This formula works for moderate to highly concentrated solutions of KCl; at low concentrations, surface conduction effects become dominant over the bulk conduction, leading to an anomalous saturation of the conductance at low salt concentration.[21] Finally, geometrical effects could also be accounted for, in particular by taking into account the hourglass-like shape of some solid-state nanopores, as shown by Kowalczyk *et al.*[22]

In this paper, we raise the question of ionic transport through an *array of multiple nanopores*. While naïve expectations would suggest that the total ion conductance G_N should scale as the number N of pores, we report experimental results for arrays with $N = 1 \ldots 50$ pores showing that the conductance per pore G_N/N *strongly decreases* with the number of pores N, with $G_N/N \to 0$ as $N \to \infty$. This result is supported by a scaling analysis of ionic transport, which is successfully compared to the experimental results. Consequences of this counter-intuitive result are discussed for ionic – but also hydrodynamic, diffusive, and thermal – transport across membranes, with implications in the context of energy harvesting.

II. FROM ONE TO TWO, TO MANY PORES: A SCALING ANALYSIS

In order to understand this prediction, we build our approach in the spirit of Hall's work.[17] The key remark made by Hille[16] and Hall[17] is that an analogy can be made between the ion transport and an electrostatic capacitance problem because the obeyed equations are identical: for ion transport, the ion current $\vec{j}$ and electric field $\vec{E}$ are connected through current conservation

$$\vec{\nabla} \cdot \vec{j} = 0, \quad \vec{j} = \kappa_b \vec{E} \tag{2}$$

leading to a Laplace equation for the electrostatic potential, as for the capacitance problem. Boundary conditions are in both case a given potential on the disk and at infinity. Consequently, the access electrical resistance for a single pore entrance is related to the capacitance C between a conducting disk of vanishing thickness, standing for the nanopore entrance, and a half-spherical electrode at infinity.[23] In mks units, this is expressed as

$$R_{\text{access}} = \epsilon \rho / C \tag{3}$$

with $\rho = \kappa_b^{-1}$ the resistivity of the medium. For a charged conducting disk of diameter d, we have[24] $C = 2\epsilon d$, leading to

$$R_{\text{access}} = \frac{1}{2\kappa_b d} \tag{4}$$

(for one side of the pore). Adding this access resistance for the two sides of the pore to the bulk resistance of a cylindrical conductor leads back to Eq. (1).

We now generalize this framework to the case of multiple pores. Following the same reasoning, the overall access resistance $R_{N,\,\text{access}}$ of the pore array can be obtained directly from the corresponding capacitance of the N conducting (and electrostatically connected) disks, as

$$R_{N,\,\text{access}} = \frac{1}{\kappa_b} \times \frac{\epsilon}{C_{\text{N pores}}} \tag{5}$$

again for one pore side.

A. Two pores

Before exploring the general N pore case, we first consider the 2-pore geometry. In this case, the calculations proceed easily by a simple electrostatic analogy. The calculation of the 2-disk capacitance separated by a distance L can be estimated recursively. We fix the potential V_0 on the disks and compute their charge. For $L \to \infty$, the charge held by each pore entrance tends to that of isolated pores, i.e., $q = 2\epsilon d V_0$. For finite L, their charge will depend on the interspacing L in order to maintain two neighboring conducting disks at the same potential, due to mutual electrostatic interaction. We make the standard simplifying assumption that the effect of a given disk on the other can be approximated by the effect of a point charge located at the center of the first disk. This assumption is expected to hold when $L \gg d$ (as may be indeed verified numerically).

In this case, the image charge $\delta q^{(1)}$ is simply $\delta q^{(1)} = -q\frac{d}{2L}$. Next orders can be calculated along the same method and within the above approximation, this leads to $\delta q^{(n)} = q \times (-d/2L)^n$, so that the total charge on a single disk is accordingly estimated by summing up all contributions as $Q = \sum_n \delta q^{(n)} = q/(1 + d/2L)$. The global access ionic resistance of the two pores is deduced accordingly

$$R_{2,\text{access}} \simeq \frac{1}{2\kappa_b\, d}\left(1 + \frac{d}{2L}\right) \tag{6}$$

and the two-pore conductance is

$$G = 2\kappa_\text{b}\left[\frac{4l}{\pi d^2} + \frac{1}{d_\text{eff}}\right]^{-1}, \tag{7}$$

where $d_\text{eff} \simeq d/(1 + d/2L)$ has the meaning of an effective electric size of the pores, modified under their mutual influence. The effective electric diameter is equal to the physical size of the pore in the absence of interpore interactions.

B. N pores: General framework

Let us generalize this result to N pores. In that case, the charge correction factor may be different for each pore, but we consider only (averaged) global properties in the present estimates. As above the conductance may be written as

$$G_N = N\kappa_\text{b}\left[\frac{4l}{\pi d^2} + \frac{1}{d_\text{eff}}\right]^{-1}, \tag{8}$$

where the effective electric size of the pore now takes the general expression

$$d_\text{eff} \equiv d \times \frac{C_{\text{N pores}}}{N C_{\text{single pore}}}. \tag{9}$$

Following the capacitance analogy, the effective electric size d_eff is defined in terms of the capacitance $C_{\text{N pores}}$ of the N pore system.

We are not aware of a general analytical estimate for $C_{\text{N pores}}$ and we therefore proceed along the same lines as for the two pore case above, with an estimate of the charge carried by each conducting disk (the pore entrances) in order to keep their potential fixed.

Using the recursive reasoning, the charge perturbations on each pore $\{\delta q_1, \ldots, \delta q_N\}$ are linearly linked to the bare charge of the pores $\{q_1, \ldots, q_N\}$

$$\delta\vec{q} = \left(-\frac{d}{2L}\right) \times \boldsymbol{A} \cdot \vec{q}. \tag{10}$$

The matrix $\boldsymbol{A}$ is a function of the geometry of the pore array. For example, for N pores in a line separated by a distance L, the matrix has the structure

$$A_{ij} = \begin{cases} 0 & i = j, \\ |i - j|^{-1} & i \neq j = 1 \ldots N. \end{cases} \tag{11}$$

The transformation matrix is always centrosymmetric in any geometry, because $A_{ij} = A_{ji}$, and in a linear geometry is also a Toeplitz matrix, which can be diagonalized numerically using fast recursive algorithms.

Now the capacitance $C_{\text{N pores}}$ follows. To first order in d/L, each pore entrance carries a total charge $Q_i \simeq q_i + \delta q_i = q_i + (-d/2L)\sum_j A_{ij} q_j$. At the zeroth order, the charges q_i are fixed by the potential V_0, as $q_i = q_0 = 2\epsilon d V_0 \,\forall i$, and the total charge in a N-pores array is

$$\begin{aligned} Q_{\text{N pores}} &\simeq \sum_i q_i - \frac{d}{2L} \times \sum_{i,j} A_{ij} q_j \\ &= 2\,N\epsilon d V_0 \left(1 - \frac{d}{2L} \times \frac{1}{N} \sum_{i,j} A_{ij}\right). \end{aligned} \tag{12}$$

Thus, we get

$$C_{\text{N pores}} \simeq N C_{\text{single pore}} \times \left(1 - \gamma_N \frac{d}{2L}\right) \tag{13}$$

with $\gamma_N \equiv N^{-1} \sum_{i,j} A_{ij}$ a global factor accounting for the geometry of the network.

We finally obtain for the effective electric size of the pores: $d_{\text{eff}} \simeq d\left(1 - \gamma_N \frac{d}{2L}\right)$. The previous expression for d_{eff} can be viewed as the first order expansion of the (physically more relevant) formula

$$d_{\text{eff}} \simeq \frac{d}{1 + \gamma_N \frac{d}{2L}}. \tag{14}$$

While this form involves a number of approximations, we anticipate from the numerical results below that this is found to agree very well with the numerical solution. Together with Eq. (8), this expression gives the conductance of the N-pore array. Note that surface conduction effects have been neglected here,[21] so that the present analysis is valid for moderate to high-salt concentrations (see Sec. IV).

C. Scaling relationships

While exact values for the geometric factor γ_N can be explicitly calculated for specific geometries, it is possible to obtain scaling relationships in the limit of a large pore array, $N \to \infty$. We consider specifically two geometries: a line of pores and 2D compact arrays, for example, made of square or triangular lattice of N pores.

The case of lines is certainly the simplest one. The corresponding transformation matrix $\boldsymbol{A}$ is given in Eq. (11) and $\gamma_N = \frac{1}{N} \sum_{i \neq j} |i - j|^{-1}$. For large N, a continuum approximation can be made and

$$\gamma_N = \frac{1}{N} \sum_{i \neq j} \frac{1}{|i - j|} \simeq \frac{1}{N} \int \int_{|x-y|>1}^{N} dx\, dy\, \frac{1}{|x - y|} \tag{15}$$

yielding

$$\gamma_N \sim \log N \tag{16}$$

for the 1D line of pores.

In the case of a 2D compact lattice of N pores, the transformation matrix $\boldsymbol{A}$ takes the generic form

$$A_{ij} = \begin{cases} 0 & i = j, \\ |r_i - r_j|^{-1} & i \neq j = 1 \ldots N, \end{cases} \tag{17}$$

with r_i the (dimensionless) positions of the pores in units of L, and

$$\gamma_N = \frac{1}{N} \sum_{i \neq j} \frac{1}{|r_i - r_j|}. \tag{18}$$

To estimate the sum in Eq. (18), we proceed using an analogy to a further electrostatic problem. The sum corresponds indeed to the electrostatic energy $\mathcal{E}_N$ of a conductor made of the N pores with unit charge. In the large N limit, a continuum approximation can be made, so that $\mathcal{E}_N = \frac{\mathcal{Q}_N^2}{2\mathcal{C}_N}$, with $\mathcal{Q}_N = N$ the total charge, and $\mathcal{C}_N$ the capacitance of the global object (here the N pores). Using standard results,[24] C_N scales linearly with the lateral size $\mathcal{R}_N$ of the compact N pores system, so that $C_N \sim \mathcal{R}_N \sim \sqrt{N}$.

Gathering results, one gets finally

$$\gamma_N \sim N^{1/2} \tag{19}$$

for 2D arrays of pores. The scaling is therefore stronger in 2D compared to the logarithmic scaling for the 1D line. This is due to the higher coordination number in 2D.

D. N-pore conductance

Altogether one therefore predicts for the conductance the following expression:

$$G_N \simeq N\kappa_b \left[\frac{4l}{\pi d^2} + \frac{1}{d} \left(1 + \gamma_N \frac{d}{2L} \right) \right]^{-1} \tag{20}$$

with $\gamma_N \sim \log N$ for lines of pores, while $\gamma_N \sim N^{1/2}$ for 2D arrays of pores.

This result demonstrates that entrance resistances do not simply add in parallel, as one would have naïvely expected. This fact is highlighted by the predicted *increase* of the factor γ_N with the number of pores N. This result stems from the long-range electrostatic interactions between pores which can never be neglected in the calculation of the global conductance of the membrane. A counter-intuitive outcome of this prediction is that – *whatever the bulk contribution to the conductance*, as described by the first term in the brackets in the right hand side of the previous equation – the contribution of entrance effects dominates for sufficiently large N and

$$\frac{G_N}{N} \propto \frac{1}{\gamma_N} \xrightarrow[N \to \infty]{} 0\,. \tag{21}$$

Entrance effects lead to a sub-linear scaling of the conductance as a function of the number of pores, and the conductance per unit pore vanishes for an infinite number of pores.

We shall come back on the astonishing consequences of this prediction in Sec. IV at the end of the paper.

E. Numerical validation

Before turning to the experimental investigation of this unexpected effect, we first validate our predictions on the basis of a numerical resolution of the transport equations using a finite-element method (COMSOL software). This allows merely to apprehend the approximations behind the above calculation.

To this end, we built up a 3D system formed by two reservoirs separated by a thin non-conducting membrane with one or N pores drilled through the membrane. We ensured that the size of reservoirs was much larger than the pore radius and the global pore array to avoid finite-size effects. We imposed an electrical potential difference ΔV between the two sides of the membrane. Then we solved the Laplace equation for the potential V, $\nabla^2 V = 0$, using a finite-element calculation. The boundary condition at the interface between the membrane and the solution is that of a vanishing flux, leading to $\vec{n} \cdot \vec{\nabla} V = 0$ on the surfaces. Finally, we measured the total ionic current I through

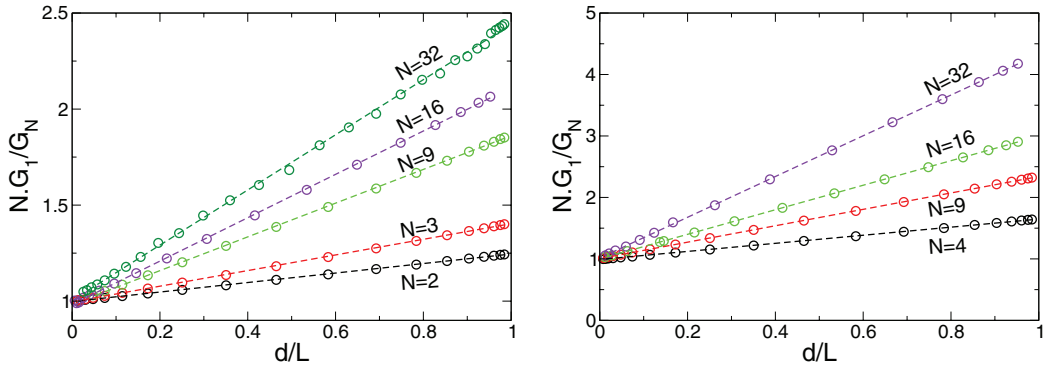

FIG. 1. Numerical results: inverse conductance for N pores, G_N, normalized by $N \times G_1$, with G_1 the conductance of a single pore, versus the inverse distance L between the pores for various numbers N of pores: (Left) N pores in a line; (right) N pores in a square array. The linear dependence does confirm the prediction in Eq. (20). The slope of the linear dependence allows to extract the geometric factor γ_N.

the pores, defined as

$$I = \kappa_b \int_S (-\vec{\nabla} V) \cdot \vec{dS} \tag{22}$$

being κ_b the bulk conductivity and S a cross-section of the system.

Within this numerical setup, we explored both the linear and 2D arrays (square and triangular lattice) for a number of pores varying from $N = 2$ up to $N = 151$ (for the triangular lattice). In Fig. 1, we show the conductance across the nanopore network, calculated numerically for a varying distance L between pores. For the various geometries, we found that the inverse conductance scales linearly with the inverse length L^{-1}, in full agreement with our main prediction in Eq. (20). This confirms thereby our prediction in Eq. (14) for the effective electrostatic diameter of the pore. The numerical computation highlights the mutual interaction of electric transport between the pores, as shown in the deformation of the electric streamlines, see Fig. 2. From the slope of the lines in the previous plot, one can accordingly extract the geometric factor γ_N. This is plotted in Fig. 3 for the line of pores, as well as for the square and triangular array of pores.

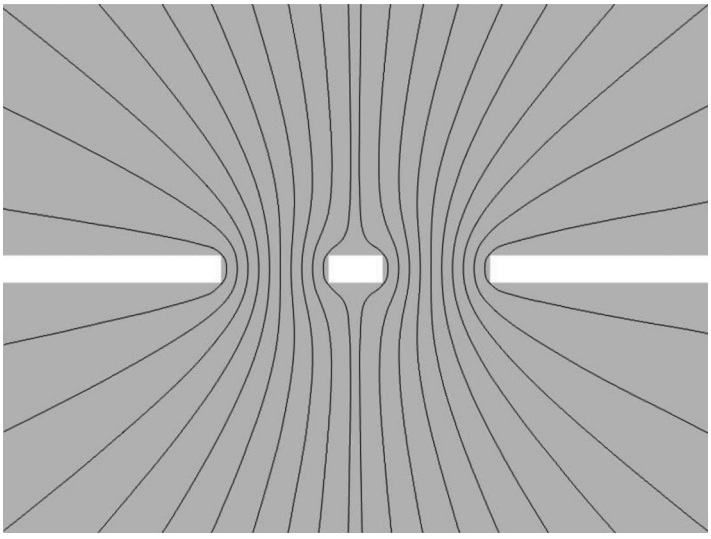

FIG. 2. Computed stream lines of the electric field, showing the deformation due to mutual interaction.

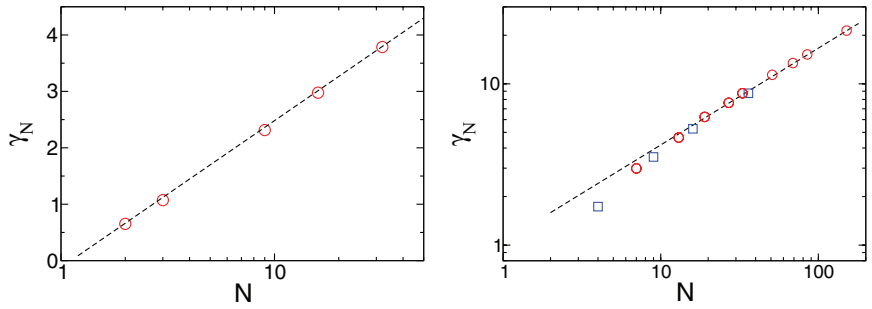

FIG. 3. Numerical results: Plot of the geometrical factor γ_N versus the number of pores N. (Left) N pores in a line: the linear fit shows that $\gamma_N \sim \log N$ in this geometry. (Right) N pores in a square array (square symbols) and in a triangular array (circle symbols). The dashed line is a power law fit with a 0.6 exponent.

Altogether these numerical calculations fully confirm the predictions of the scaling analysis. The geometric factor is found to scale logarithmically in N for the linear array, $\gamma_N \sim \log N$, while it scales algebrically with the number of pores in the 2D system, $\gamma_N \sim N^{\alpha}$, with a measured exponent $\alpha \simeq 0.6$ very close to the predicted one (0.5). We attribute the slight difference in exponent in edge effects which should disappear in the very high N regime (which we could not reach numerically).

III. LINEAR AND SQUARE ARRAYS OF PORE: EXPERIMENTAL RESULTS

We now turn to the experimental counterpart with the aim to explore the electric conductance across an array of nanopores.

A. Fabrication process and experimental protocol

To fabricate multipore membranes, we used 50 nm-thick silicon nitride (Si_3N_4) membranes drilled by Focused Ion Beam (FIB) milling. The resulting nanopores were cylindrical, with diameter $d \approx 200$ nm. Various FIB scan protocols were tested in order to obtain straight cylinders. Using this technique, we fabricated membranes with 1–90 drilled nanopores in a line or in square array, with various distances L between the pores. The actual distances and diameters were measured post-fabrication by SEM imaging, with errors of a few nanometers. Figure 4(b) shows the SEM image of a sample with various nanopore arrays.

Each membrane was then inserted in a custom-made electrochemical cell between two reservoirs of a KCl solution of concentration c_s, made from deionized water and solid KCl (*Acros Organics*, 99% purity), see, e.g., Ref. 21. The conductivity of the solution was checked before and after each experiment with a conductimeter (HI 2550, *Hanna Instruments*), and no particular drift was observed.

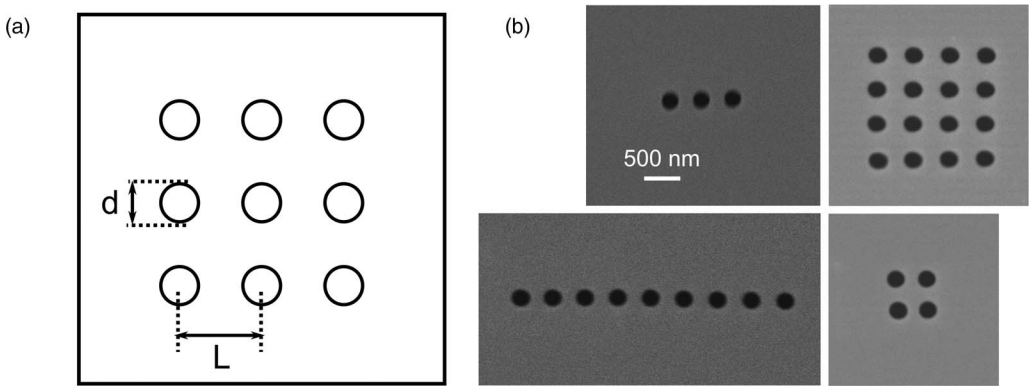

FIG. 4. (a) Sketch of the system. (b) SEM images of FIB-milled multipores: pore lines and square arrays.

The conductance of the nanopores was extracted from I-V characteristic curves, measured with a custom-made I/V converter and a National Instruments DAQ board, using Ag/AgCl electrodes.

B. Three pores in a line

We first explore the case of three pores in a line, which we compare to the measurements obtained for a single-pore membrane. Figure 5 reports the dependence of the conductance for the 3-pore system as a function of the distance L between the pores. While the conductance normalized to its single pore value, $G_3/3G_1$, approaches unity when $L \gg d$, a strong decrease of the multipore conductance, with respect to the sum of the contributions of individual pores, is observed at small interpore distance $L \approx d$, so that $G_3 < 3 \times G_1$. Furthermore, the theoretical prediction in Eq. (20) is found to reproduce fairly well the experimental results (with $\gamma_3 = 1.07$ as obtained from the numerical calculation).

C. Multipore arrays: Linear and square geometries

While the above experiment confirms the strong mutual influence of the nanopores, our focus is merely on the dependence on the number of pores N. To this end, we have measured the conductance in (linear and square) arrays of nanopores, with a number of pores varying between $N = 1$ and $N \approx 50$ for a given interpore distance L ($L \approx 2\,d$). The results are displayed in Fig. 6. The conductance of the multipore system G_N, normalized by N times the expected contribution of an individual pore, is plotted versus the number of pores N. The panels (a) and (b) of this figure clearly demonstrate that the normalized conductance G_N/N *decreases* by a large factor with the number of pores N.

As suggested by our prediction in Eq. (20), these data are presented in the panels (a′) and (b′) as NG_1/G_N versus N to highlight the scaling behavior of the entrance effects. The results for the line of nanopores, panel (a′), do exhibit a $\log N$ scaling, in full agreement with our predictions above. The 2D square array exhibits a slow algebraic increase of the entrance effects, as highlighted by the comparison to a $N^{1/2}$ scaling in panel (b′), again in agreement with our predictions. Altogether the experiments fully confirm the sublinear scaling of the conductance due to entrance effects.

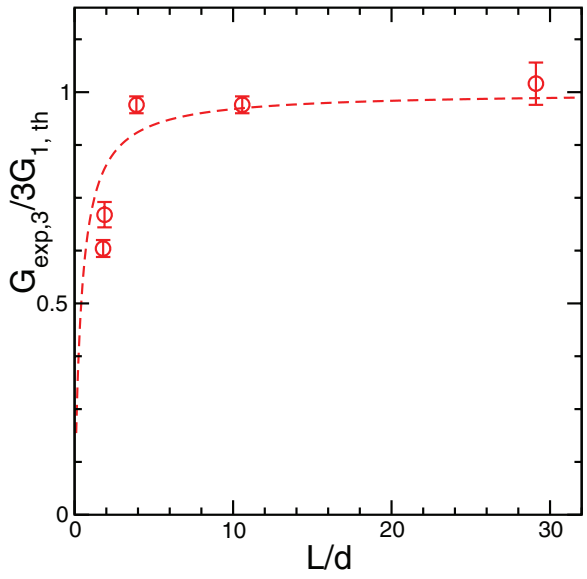

FIG. 5. Experimental values of the normalized conductance $G_3/3G_1$ of 3-nanopores linear arrays, with G_3 measured conductance of the sample and $G_{1,\,\mathrm{th}}$ the predicted conductance of a single nanopore, as a function of the normalized distance L/d. The pore diameter is $d = 226$ nm. Error bars are obtained from measurements over various realizations and 5 salt concentrations in the range $10^{-2} - 1$ M. The dashed line is the prediction using Eq. (20) (with $\gamma_3 = 1.07$ as obtained from the numerical calculation).

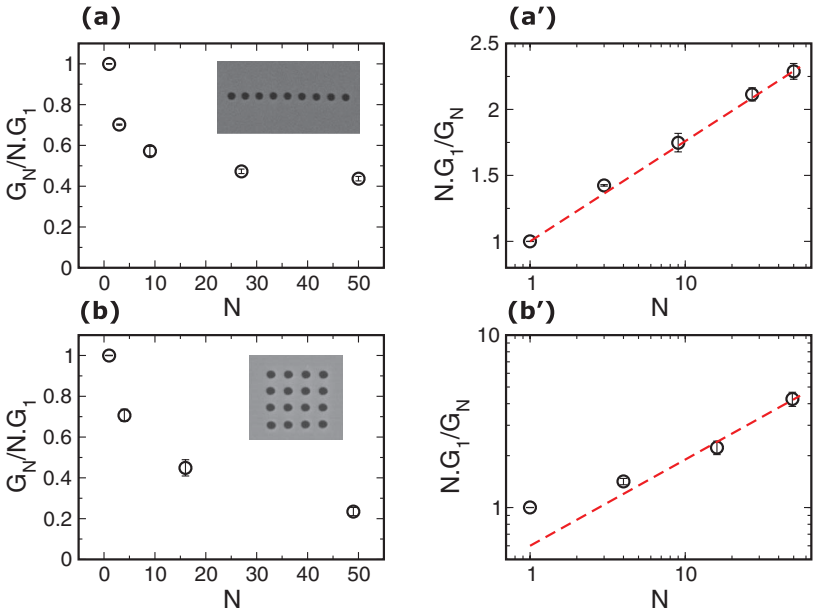

FIG. 6. Experimental results: conductance across N nanopores in a line (a) and in a square array (b), as a function of the number of nanopores N. The conductance is normalized by N times the value expected for a single nanopore. The distance between nanopores is fixed $L \approx 2\,d$ (with $d \approx 200$ nm the pore diameter). In panels (a′) and (b′), the inverse conductance is plotted versus the number of pores in order to highlight the scaling with N. The dashed line highlights the predicted $\log N$ behavior for the linear geometry (panel (a′)), while it shows a $N^{1/2}$ scaling for the square geometry (panel (b′)). This plot gathers measurements for salt concentration C_s between 10^{-2} and 10^{0} M, as the normalized conductance is independent of concentration in this regime.

IV. DISCUSSION

In conclusion, we experimentally demonstrated and theoretically justified that the conductance through arrays of nanopores exhibits an anomalous sub-extensive dependence of the conductance on the number of pores. The total ion conductance normalized by the sum of individual contributions *strongly decreases* with the number of pores N. A theoretical framework shows that this counter-intuitive behavior originates in the mutual interactions between the nanopores. The long range nature of the transport leads to a bending of the field lines at pore entrances, thereby modifying the apparent cross section of each pore.

We furthermore proposed a scaling approach showing that the global entrance effects diverge as N goes to infinity. This leads to a sublinear dependence of the total conductance versus the number of pores, scaling as $G_N \sim N/\log(N)$ for an array of N pores in a line, and $G_N \sim N^{1/2}$ for a 2D array of pores. An astonishing consequence is that the normalized conductance G_N/N *vanishes* for an infinite number of pores, $G_N/N \to 0$ as $N \to \infty$. We checked this result by finite-element simulation, finding a good agreement with experimental results.

We quote that our results are valid in the regime where the surface conduction can be neglected as compared to the bulk conduction inside the pore. This corresponds to a regime where the so-called Dukhin length, ℓ_D, defined as the ratio between surface and bulk conductance, is smaller than the interpore distance. Indeed, as shown in Ref. 21, the surface conduction inside the pore is expected to modify the electric field lines up to a distance ℓ_D in the bulk and the interactions between pores would be modified when ℓ_D compares with the interpore distance. This effect has not been considered in our description, and our approach is accordingly valid for negligible surface conduction. This implicitly assumes moderate to high salt concentration. It would be however highly desirable to extend our predictions to include the effects of surface conduction.

The consequences of this result are highly non-trivial. It shows that the total conductance of a 2D array of pores scales sub-extensively with the number of pores due to entrance effects and

multipore interactions, so that in the macroscopic scale, $G_N \propto \sqrt{N} \times \kappa_b L$ as $N \to \infty$ (L the interpore distance).

The result bares some similarity with the collective sedimentation of particles.[25] Beyond its vectorial nature, the Navier-Stokes equation exhibits a similar laplacian form (for the pressure equation), leading to long-range hydrodynamic interaction between the particles. It is known in this context that sedimentation exhibits very strong finite-size effects.[25,26] Our prediction is a counterpart of this behavior for electric transport.

The anomalous scaling of the conductance originates from entrance effects. As it can be seen from our main prediction in Eq. (20), entrance effects always prevail over bulk conductance through the membrane for sufficiently large N. Typically this occurs – using Eq. (20) – when $\gamma_N \gtrsim L \cdot l/d^2$, with l and d the length and diameter of the pores, and L their interdistance. This condition occurs above a threshold number of pores, $N^\star$. For a 1D line of nanopores, $N^\star \approx \exp[L \cdot l/d^2]$, while $N^\star \approx (L \cdot l/d^2)^2$ for a 2D array. Above $N^\star$, entrance effects start to play a dominant role and the anomalous scaling for the conductance is in effect, decreasing the conductance with the number of pores N. For membranes made of pores with large aspect ratio $l/d \gg 1$, $N^\star$ is accordingly very large and the effect is weak. However, for thin membranes with a pore aspect ratio smaller than one, $N^\star$ is typically of order unity and the sub-linear scaling should show up as in the present measurements.

This counter-intuitive result raises a number of questions for electric transport across membranes, as it shows that for sufficiently large areas, the entrance effects dominate over the resistance inside the pores. In any case, these effects will be particularly dominant for ultrathin membranes, such as graphene pierced by many pores. While one would naïvely expect that, for the molecularly thin graphene layer, a huge electric potential gradient should build up across the membrane, our results do show in contrast that interactions between pores should decrease strongly the corresponding ionic transport across this ultrathin membrane.

Furthermore, it is also interesting to note that the theoretical framework proposed here can be easily generalized to any transport phenomena involving a laplacian type of equation. This is due to the conservation equation which leads to long-range interaction between the pores. While this should deserve further systematic investigations, the present results are expected to generalize to hydrodynamic transport, as well as diffusive or heat transport (provided the membrane is assumed to be thermally insulating). This raises accordingly the question of finite size effects on the global permeability of thin membranes, as well as the diffusive permeability of such membrane to solutes. Such questions would deserve a much more detailed investigation in the context of reverse osmosis and desalination process. The consequences are numerous and quite subtle. For example, due to the large entrance resistance, the potential drop inside the pore is substantially smaller. So this should impact any transport phenomena taking its origin in the corresponding driving force. This is in particular the case of cross transport phenomena, such as electro-osmosis. Due to Onsager symmetry, the same applies to the streaming current, which is the electric current induced by hydrodynamic flow under a pressure drop. This incidently confirms that the effects discussed here for electric transport should apply for hydrodynamic transport as well. A strong hydrodynamic resistance at the entrance leads to a smaller pressure drop inside the pore, thereby reducing corresponding fluxes (mass and electric).

In the context of energy harvesting, streaming currents were considered as an interesting new route to produce electric current I_{stream} from pressure gradients.[27] The maximum power produced is easily calculated as $\mathcal{P}_{\max} = \frac{1}{4} G^{-1} \times I_{\text{stream}}^2$, with G the global conductance of the membrane. Due to the anomalous entrance effects, the conductance will decrease with the number of pores, and this may be thought as a strong amplification factor for the produced power. However, as discussed above, the current I_{stream} is proportional to the pressure gradient inside the pore, $I_{\text{stream}} \propto [\nabla P]_{\text{in}}$, which is also affected by the same entrance effects, with similar scalings as for the conductance. Altogether this should therefore lead to a *decrease* of the produced power as a function of the number of pores, with similar scaling laws as discussed in the present article.

Such effects may however be circumvented for the alternative diffuso-osmotic energy harvesting under salt concentration gradients,[28] whereby an electric current is generated by a salt concentration gradient, $I_{DO} \propto \nabla C_{\text{salt}}$. Indeed, while the salt concentration gradient inside the pore should *a priori* be affected by similar effects, the possibility of convective mixing of the salt may allow to bypass

the limitations induced by mutual effects between pores in diffusive transport (while keeping the effect for the electric conductance). In this case, the corresponding generated power – similar to the case of streaming currents – may be therefore increased due to the corresponding decrease of the conductance.

Altogether, entrance effects across membranes exhibit subtle and counter-intuitive features, which – provided they are used properly – can be harnessed for applications in various fields.

ACKNOWLEDGMENTS

The authors acknowledge financial support from ERC-AG project *Micromegas*. A.G. and A.S. thank G. Ferrini for assistance with computer algebra software. We thank R. Brossard for his help in the experiments. Many fruitful discussions with A.-L. Biance and L. Joly are acknowledged.

[1] C. Dekker, "Solid state nanopores," Nat. Nanotechnol. **2**, 209 (2007).
[2] T. Humplik, J. Lee, S. C. O'Hern, B. A. Fellman, M. A. Baig, S. F. Hassan, M. A. Atieh, F. Rahman, T. Laoui, R. Karnik, and E. N. Wang, "Nanostructured materials for water desalination," Nanotechnology **22**, 292001 (2011).
[3] W. Guo, L. Cao, J. Xia, F.-Q. Nie, W. Ma, J. Xue, Y. Song, D. Zhu, Y. Wang, and L. Jiang, "Energy harvesting with single-ion-selective nanopores: A concentration-gradient driven nanofluidic power source," Adv. Funct. Mater. **20**, 1339 (2010).
[4] M. Napoli, J. C. T. Eijkel, and S. Pennathur, "Nanofluidic technology for biomolecule applications: A critical review," Lab Chip **10**, 957 (2010).
[5] S. Howorka and Z. S. Siwy, "Nanopore analytics: Sensing of single molecules," Chem. Soc. Rev. **38**, 2360 (2009).
[6] Z. S. Siwy and S. Howorka, "Engineered voltage-responsive nanopores," Chem. Soc. Rev. **39**, 1115 (2010).
[7] O. A. Saleh and L. L. Sohn, "Direct detection of antibody-antigen binding using an on-chip artificial pore," Proc. Natl. Acad. Sci. U.S.A. **100**, 820 (2003).
[8] N. Durand and P. Renaud, "Label-free determination of protein-surface interaction kinetics by ionic conductance inside a nanochannel," Lab Chip **9**, 319 (2009).
[9] I. Vlassiouk, P. Y. Apel, S. N. Dmitriev, K. Healy, and Z. S. Siwy, "Versatile ultrathin nanoporous silicon nitride membranes," Proc. Natl. Acad. Sci. U.S.A. **106**, 21039 (2009)
[10] C. C. Striemer, T. R. Gaborski, J. L. McGrath, and P. M. Fauchet, "Charge- and size-based separation of macromolecules using ultrathin silicon membranes," Nature (London) **445**, 749 (2007).
[11] M. Wanunu, W. Morrison, T. Rabin, A. Y. Grosberg, and A. Meller, "Electrostatic focusing of unlabelled DNA into nanoscale pores using a salt gradient," Nat. Nano **5**, 160 (2010).
[12] G. F. Schneider, S. W. Kowalczyk, V. E. Calado, G. Pandraud, H. W. Zandbergen, L. M. K. Vandersypen, and C. Dekker, "DNA translocation through graphene nanopores," Nano Lett. **10**, 3163 (2010).
[13] S. Garaj, W. Hubbard, A. Reina, J. Kong, D. Branton, and J. A. Golovchenko, "Graphene as a subnanometre trans-electrode membrane," Nature (London) **467**, 190 (2010).
[14] S. C. O'Hern *et al.*, "Selective molecular transport through intrinsic defects in a single layer of CVD graphene," ACS Nano **6**, 10130 (2012).
[15] D. Cohen-Tanugi and J. C. Grossman, "Water desalination across nanoporous graphene," Nano Lett. **12**, 3602 (2012).
[16] B. Hille, "Pharmacological modification of the sodium channels of frog nerve," J. Gen. Phys. **51**, 199 (1968).
[17] J. E. Hall, "Access resistance of a small circular pore," J. Gen. Phys. **66**, 531 (1975).
[18] I. Vodyanoy and S. M. Bezrukov, "Sizing of an ion pore by access resistance measurements," Biophys. J. **62**, 10 (1992).
[19] P. Läuger, "Diffusion-limited ion flow through pores," Biochim. Biophys. Acta **455**, 493 (1976).
[20] M. Aguilella-Arzo, V. M. Aguilella, and R. Eisenberg, "Computing numerically the access resistance of a pore," Eur. Biophys. J. **34**, 314 (2005).
[21] C. Lee, L. Joly, A. Siria, A.-L. Biance, R. Fulcrand, and L. Bocquet, "Large apparent electric size of solid-state nanopores due to spatially extended surface conduction," Nano Lett. **12**, 4037 (2012).
[22] S. W. Kowalczyk, A. Y. Grosberg, Y. Rabin, and C. Dekker, "Modeling the conductance and DNA blockade of solid-state nanopores," Nanotechnology **22**, 315101 (2011).
[23] It has to be noted that, in practice, entrance effects can be eliminated if the electrodes are positioned at the pore entrances, e.g., by patterning metal directly on the membrane. The assumption of hemispherical electrodes at infinity is suitable to the common experimental case of macroscopic electrodes inserted into large solution reservoirs, and therefore ignores any possible finite-size effects.
[24] J. D. Jackson, *Classical Electrodynamics* (Wiley, New York, 1962).
[25] G. K. Batchelor, "Sedimentation in a dilute dispersion of sphere," J. Fluid Mech. **52**, 245 (1972).
[26] R. E. Caflisch and J. H. C. Luke, "Variance in the sedimentation speed of a suspension," Phys. Fluids **28**, 759 (1985).
[27] F. H. J. van der Heyden, D. J. Bonthuis, D. Stein, C. Meyer, and C. Dekker, "Electrokinetic energy conversion efficiency in nanofluidic channels," Nano Lett. **6**, 2232 (2006); "Power generation by pressure-driven transport of ions in nanofluidic channels," *ibid.* **7**, 1022 (2007).
[28] A. Siria, P. Poncharal, A.-L. Biance, R. Fulcrand, X. Blase, S. Purcell, and L. Bocquet, "Giant osmotic energy conversion measured in a single transmembrane boron nitride nanotube," Nature (London) **494**, 455 (2013).